Send Orders for Reprints to reprints@benthamscience.ae

Protein & Peptide Letters, 2016, *23*, 217-231

A Brief Survey of State-of-the-Art BioSAXS

Thomas Bizien[a], Dominique Durand[b], Pierre Roblin[a,c], Aurélien Thureau[a], Patrice Vachette[b] and Javier Pérez*[a]

[a]*Beamline SWING, Synchrotron SOLEIL, Saint-Aubin, France;* [b]*I2BC, Université Paris-Saclay, Orsay, France,* [c]*CEPIA, INRA Nantes, France*

Javier Perez

Abstract: In the field of structural biology, Small Angle X-ray Scattering (SAXS) has undergone a tremendous evolution in the last two decades. From a craft reserved to a few experts in the late 80's, it has now turned into a high-throughput technique, following the same trend as macromolecular crystallography. Synchrotron radiation has played a key role in this evolution, by providing intense X-ray beams of high optical quality that made possible the recording of statistically meaningful data from weakly scattering biological solutions in a reasonable time. This, in turn, prompted the development of powerful and specific software for data analysis and modeling. In this mini-review, mainly addressed towards a broad readership, representing as many potential users, we try to summarize the latest aspects of evolution of BioSAXS, both conceptually and from the point of view of instrumentation. We emphasize the need for complementary experimental or computational techniques used in combination with SAXS. The great potential of these multi-pronged approaches is illustrated by a series of very recent studies covering the various ways and means of using BioSAXS.

Keywords: Beamline, biological macromolecules, conformation, hybrid methods, small-angle X-ray Scattering, solution, structure.

1. INTRODUCTION

Small Angle X-ray Scattering (SAXS) is a simple and powerful technique that directly provides structural information at scales ranging typically from 1 nm to 1 µm. Discovered as a side-effect of diffraction patterns in the late 30's, its theory and instrumentation were developed during the following decades with scientific focus in the fields of material science and soft condensed matter [1-3]. The physical principle is the same as that of X-ray crystallography, based on elastic scattering of an incoming X-ray wave by the electrons of the sample. The output is a scattering pattern most frequently collected using a bi-dimensional detector positioned behind the sample and perpendicular to the incoming beam. The symmetry of the scattering pattern directly depends on the internal symmetry of the sample, e.g. an isotropic liquid sample gives rise to a scattering pattern with circular symmetry. The collected intensity is proportional to N, the number of objects within the sample. It directly results from their size, shape and internal structure, through the Fourier Transformation modulus of their electronic density, given here for an isotropic sample:

$$I(q) = r_e^2 \sum_{p=1}^{N} \left\langle \left| \iiint_{V_p} (\rho_e(\vec{r}) - \rho_0) e^{-i\vec{q}\cdot\vec{r}} d^3r \right|^2 \right\rangle_\Omega \qquad \text{Eq 1}$$

where the triple integral is performed within the volume V_p of each particle and the average performed over all possible orientations Ω. r_e is the classical electron radius, $\rho_e(\vec{r})$ is the electronic density at position $\vec{r}$ within the particle, ρ_0 is the *average* electronic density of the surrounding buffer (or matrix), $q = \frac{4\pi \sin(\theta)}{\lambda}$ is the momentum transfer, 2θ is the scattering angle, typically below a few degrees, and λ is the X-ray wavelength. The rotational average severely limits the structural information content of the scattering pattern obtained in a SAXS experiment. Application of SAXS to biology remained a lesser known and marginal area of structural biology before the 90's when the introduction of software programs that could relate the atomic structure of a macromolecule to a SAXS experimental pattern with unprecedented ease and accuracy [4] together with the availability of powerful synchrotron beams [5] triggered a considerable and continuing development. BioSAXS possesses its own procedures in data treatment and analysis, rather different from those of conventional SAXS, due to the fact that solutions of biological macromolecules and complexes contain strictly identical particles in contrast to the size distribution inherent to synthetic materials. As testified by the large number of recent reviews [6-10], it has evolved into an extremely popular method amongst structural biologists, as a strongly advisable complement to high resolution studies, e.g. crystallography, NMR, electron microscopy (see [11] for a thorough, up-to-date, comprehensive report on BioSAXS). Besides being a strong experimental constraint for high-resolution modeling in solution, BioSAXS can provide direct information about the size and shape of macromolecules in solution with no need for any model. Radius of gyration, R_g, molecular mass, M, and intramolecular pair-distribution function, P(r) (i.e. the distribution of all distances between

*Address correspondence to this author at the Beamline SWING, Synchrotron SOLEIL, Saint-Aubin, France; Tel: +33(0) 169359619;
E-mail: javier.perez@synchrotron-soleil.fr

1875-5305/16 $58.00+.00

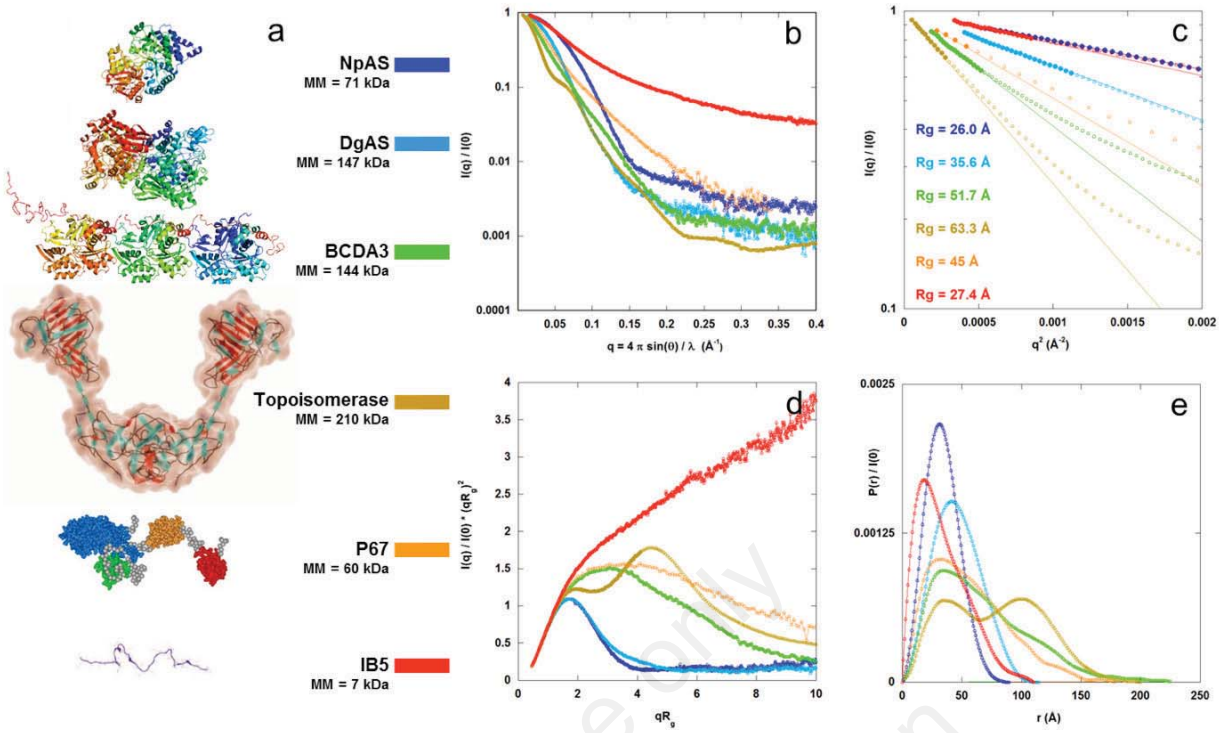

Figure 1. SAXS curves from a selection of different protein structures.
a: A 3D representation of the selected proteins, whose structures fit the BioSAXS data; NpAS [18] (PDB ID 1G5A); DgAS [18] (PDB ID 3UER); BCDA3 (unpublished construct, based on actin [19] PDB ID2ZWH); Topoisomerase [20] (PDB ID 2ZBK); P67 [21]; IB5 [22].
b: The usual representation of a SAXS pattern, I(q) *vs* q in log scale, normalised to 1 at q=0.
c: The Guinier Plot, I(q) *vs* q^2 in log scale, displays a negative linear slope at small q values directly proportional to R_g^2.
d: The dimensionless Kratky Plot, $I(q)/I(0)\times(q\times R_g)^2$ *vs* $q\times R_g$, is extremely useful to distinguish between different degrees of folding. Proteins containing folded domains display a bell shaped curve, whith a maximum of about 1.1 at around q.Rg=1.75. With increasing elongation and degree of unfolding, the curve maximum shifts to the upper right and the slope of the right side of the curve increases.
e: The distance distribution function, P(r), directly derived from the previous curves using programs such as Gnom [23], and normalized to I(0). The maximum extension, D_{max}, of the P(r) corresponds to the maximum spatial extension of the protein. An asymetric P(r), with a sharp peak at small r-values that extends far towards the high r-values is usually representative of an elongated protein, as is the case for BCDA3, P67 and IB5. Local maxima in the P(r) reflect the existence of well separated domains in the protein, as is the case for Topoisomerase.

any pair of points within the particle), can be directly derived from the experimental data, using the Guinier equation $I(q) \cong I(0)e^{\frac{q^2Rg^2}{3}}$ at very small angles, semi-empirical calculations of the Porod volume or the correlation volume, and indirect Fourier Transformation, respectively. Beginners may find a very clear hands-on introduction to all these notions in the paper by Jacques *et al.* [12], together with a series of pitfalls to avoid in the data analysis. More advanced introductions to BioSAXS can be found in [13-15]. In complement to the above-mentioned structural outputs, the dimensionless Kratky-Porod plot is an additional tool to derive qualitative information about the degree of compactness of a protein [16,17]. Figure **1** presents the typical output from a BioSAXS acquisition and the main ways to obtain immediate structural information.

2. STRUCTURAL OUTPUT FROM BIOSAXS

As already hinted to in the introduction, the structural information content of a scattering curve is very limited. This explains why it is necessary to use each available piece of information for data interpretation and modeling and/or to complement SAXS with other approaches. This is why the program Crysol [4] (1995) marked a turning point in the field as it opened the way to what are now known as hybrid methods in which the available high resolution structures of domains (case of a multi-domain protein) or isolated partners (case of a complex) together with all kinds of local information are harnessed to the interpretation of the SAXS data. The problem addressed by Crysol is recapitulated in Equation 2 that expresses the intensity scattered by identical, non-interacting macromolecules in solution as a function of their intramolecular atomic distances:

$$I(q) = N\, r_e{}^2 \left\{ \sum_{i=1}^{Nat} \sum_{j=1}^{Nat} \Delta f_i(q) \Delta f_j(q) \frac{sin(q d_{ij})}{q d_{ij}} + h_{ij}(q) \right\} \qquad (2)$$

where the double sum is the Debye equation, $h(q)$.is the *hydration layer contribution*, d_{ij} is the distance between any pair of atoms (i,j), $\Delta f_i(q) = f_i(q) - g_i(q)$ is the atomic contrast form factor, $f_i(q)$ is the (known) atomic form factor and $g_i(q)$ is the (empirical) excluded volume form factor. Although Equation 2 is definitely accepted, there has been intense de-

bate about the appropriate derivation of the contrast and hydration layer contributions, $g_i(q)$ and $h_{ij}(q)$, both of which have traditionally included a coefficient used as a fitting parameter. This was actually the case of Crysol, which described hydration water as a continuous, homogeneous, 3 Å-thick layer of water with a different electron density than bulk water. This is also true for FoXS that adjusts the scattering factor of surface atoms as a function of their exposure to solvent [24] (http://modbase.compbio.ucsf.edu/foxs/). A new and very promising approach has been proposed a few years ago to avoid these uncertainties by exploiting all-atom molecular dynamics calculations of the macromolecule together with explicit surrounding buffer molecules. This sustained effort by several groups has recently culminated in a program made publicly available on a dedicated website (see [25] and references therein, http://waxsis.uni-goettingen.de/). Confirmation of the robustness of this protocol in the coming years will certainly help to put BioSAXS on even firmer grounds.

In view of the limited resolution of the SAXS data, all modeling algorithms preserve the detailed structure of individual domains or partners in a complex. The program SASREF from the ATSAS package that can simultaneously fit the ensemble of scattering patterns of partial complexes if available, uses three rotation and three translation parameters to describe the rigid body movements of each subunit [26]. The implicit assumption is that there is no significant conformational change of subunits between the isolated state, in a partial complex and within the full complex under study. In the case of multi-domain proteins comprising well-structured domains linked by unknown, possibly flexible linkers, the latter may be described as chains of Dummy Residues (DR) - spherical scattering element centered at the Cα position and possessing the scattering factor of an average residue- as implemented in the program BUNCH from the ATSAS package [26]. More recently, the program CORAL [27] was developed that handles several chains as does SASREF while being able to describe missing parts as does BUNCH. The approximation involved in the use of DRs can be partially overcome by subsequent replacement of DRs by a full atom description using the routine PD2 [28] before final calculation of the scattering pattern of the substituted model. Other programs such as AllosModFoXS [29] (from the IMP package, http://modbase.compbio.ucsf.edu/allosmod-foxs/), Bilbo-MD [30] (http://bl1231.als.lbl.gov/bilbomd), Dadimodo [31], SASSIE [32] and Xplor-NIH [33] directly work on an all-atom description at all stages of the model "refinement". At the cost of a larger computing time, the main advantage of such approaches is two-fold: first, the accurate description of the residues justifies fitting the curve to higher q-values, thus allowing a full use of the experimental data; second, a plausible stereochemistry of the unknown residues is permanently maintained by the use of a molecular dynamics force field.

In the case where no high resolution information is available, other approaches, the so-called *ab initio* methods, have been developed. Here, the particle is described as a compact ensemble of identical spheres, termed dummy atoms (DA), the scattering of which is as close as possible to the experimental curve. Since all spheres are identical, their assembly yields a uniform volume that only accounts for the shape of the object without any inner density inhomogeneity. This approximation only holds true at very low resolution. This algorithm has been implemented in the program DAMMIN [34] and its recent, much faster version DAMMIF [35]. The program DENFERT uses a similar approach but also includes explicitly the hydration layer modeled as DA's of a different density [36]. A multiphase version of DAMMIN in which each homogeneous phase is attributed its own electron density contrast has been implemented in the program MONSA [27], an example of which is presented below in the section dedicated to the study of complexes. Finally, the program GASBOR uses another description of a protein as a chain of N dummy residues where N is the number of amino-acid residues [37]. In all cases, these heuristic, Monte-Carlo based modeling approaches require performing tens of runs before analysis of the ensemble of models extracts the common properties to all models from meaningless details of each individual shape. Models derived using GASBOR and MONSA are shown in the case of complex structures presented below. In both cases, however, the biological relevance entirely relies on the accompanying hybrid model.

We wish to conclude this section with a word of caution regarding a frequent use of *ab initio* models where atomic models are superimposed into the resulting volume, probably inspired by a classical approach in the apparently similar situation of low resolution electron microscopy. However the similarity between the electron density map from EM and the SAXS derived shape (or DR model) is only apparent. Many EM images and extensive processing yield one model recapitulating all the available structural information. In contrast, from a unique, well-defined SAXS pattern, many shapes, each of them fitting the experimental curve equally well, can be recovered. In favorable cases, they can be grouped in a unique family but, often, several clusters can be defined in the solution space. The superimposition of individual domain or partner structures into the complex volume is thus far from being unambiguous and is therefore of limited informative value, with a clear risk of producing erroneous arrangements. At the very least, the scattering pattern of the resulting arrangement of domains should be calculated and compared with the experimental data for validation. In spite of this obvious shortcoming, it is widely used, probably due to its direct appeal to the reader and its simplicity of use. Much to be preferred is the use of hybrid methods, *i.e.* directly fitting the scattering curve.

3. INSTRUMENTATION

A list of synchrotron beamlines where an important part of beam time and conception efforts are devoted to biological solution SAXS has been recently reported [8]. Weakly concentrated biological samples (*e.g.* from 0.1 to 10 mg/ml) mostly require a high flux and parallel beam, and a low background detector. Without doubt, the most important technological improvement in recent years came from the new generation of hybrid pixel X-ray detectors, that have enhanced the signal to noise ratio dramatically with very low dark count rates [38,39]. Practically, such detectors have reduced by at least an order of magnitude the lowest concentration compatible with useful data recording. Operating the detector in vacuum also helps to reduce X-ray absorption

[40,41] and makes it very easy to change the sample-to-detector distance. Absorption by air and parasitic scattering arising from slits, on-path windows and sample holders need also to be reduced to a minimum for weakly scattering samples. Measurement cells have been designed to operate in vacuum [40-43]. When the sample holder is in air, the material of the X-ray windows closing the in-vacuum flight tubes must be optimized to reduce parasitic scattering while maintaining a strong resistance to differential pressure [44-46]. The material and the geometry of the blades that are used to collimate and "shape" the main beam have also been considerably improved [47]. On the Australian SAXS beamline, hybrid germanium single crystals in the anti-scatter and guard slits combined with a small active beam-stop have proved to considerably enhance the reproducibility and quality of the alignment [45].

Hardware improvements have also been made during the last decade to increase the rate of sample turnover [48-51]. Thanks to dedicated sample-changer robots, the typical time between two sample injections has been drastically reduced down to between 1 to 5 minutes, with small amounts of sample injected (between 10 and 50 µl), and including a cleaning sequence. Automation clearly reduces human errors and allows for many conditions to be tested rapidly. The high-throughput strategy is of course optimally beneficial when pure and monodispersed samples are used, but also provides one with the opportunity of evaluating non-optimized samples. Combination of SAXS with on-line Size-Exclusion Chromatography (SEC) is an alternative strategy, now also installed at many beamlines (Figure **2**). With a single sample injection, a buffer curve whose composition is necessarily identical to that of the sample is obtained together with a series of sample curves at different concentrations. The possible presence of aggregates, one of the main problems in BioSAXS, potentially giving rise to wrong interpretations, is not an issue anymore, since these are kinetically separated from the sample of interest by the SEC elution process. Strong complexes can be separated from their individual partners, and even weak complexes can be analyzed, provided the equilibrium is shifted towards complex formation by adding an appropriate amount of one of the partners in the elution buffer composition [52]. Using small and performant SEC columns, with smaller size beads resulting in higher flow rates and better resolutions, elution times have been considerably reduced. Acquisitions every 20 min are now common at the SWING beamline by alternating between two separated elution circuits. SEC-SAXS in turn prompted software developments to automatize data processing and to try and improve the decomposition of the recorded dataset into the scattering patterns of not fully resolved species [53-55].

Microfluidic devices have also been recently designed to reduce sample consumption and to screen a wide set of conditions [56]. They have been used to monitor structural changes in response to buffer exchange or to variation of protein concentration [57], to study aggregation and fibre formation [58] or to screen different protein concentrations with different buffer composition [41]. These devices require a very low amount of sample and buffer (2 to 5µL) and might become standard on Biological SAXS beamline in the future.

With the high data rates imposed by the high–throughput methods, automated software pipelines for data reduction and analysis became essential [59-61]. The main objective is to make BioSAXS data analysis as easy and straightforward as possible for non-experts biologist users. IspyB is an example of a graphical tool jointly developed by several synchrotron facilities in Europe to display the processed results in a unified way [62]. The challenge for experts is now to improve the ability of these pipelines to provide a correct interpretation of the data, and detect poor quality samples. In complement, training the non-expert users through the use of a more hands-on application that goes interactively through the whole process might be beneficial to BioSAXS by increasing the ability of the general user to evaluate the quality of recorded data.

4. COMPLEXES

The modeling process in the case of complexes, protein/protein or protein/nucleic acid alike, must always be adapted to the specific case under study. However, a few general rules should be obeyed that are summarized below:

SEC-SAXS measurements are to be preferred if at all possible, in order to obtain the scattering pattern of the complex free from contributions from isolated partners [63]. It is particularly important in the case of low affinity complexes, provided one (the smallest partner) of the partners is added to the elution profile so as to avoid dissociation during elution [52].

All available high resolution structures of partners are to be taken into account. Missing residues should be completed using the scattering curves of isolated partners and the programs BUNCH and SASREF [26] (see the ATSAS package), AllosModFoXS [29,64] (from the IMP package http://www.salilab.org/imp/) or SASSIE [32]. If no atomic structure is available, a homology model may be built using one of the many available tools.

Of utmost importance is the information about the regions of interaction. These might be obtained from complementary biochemical studies; for instance systematic study of mutant proteins. Cross-linking experiments coupled to Mass Spectrometry analysis can also be very informative, as can be SHAPE footprinting [65] as well as CRAC and CLIP methods in the case of protein/RNA complexes [66]. This information is crucial to constrain the solution space for partners' arrangement in the complex.

NMR experiments are perfectly complementary to SAXS (for a revue, see [67]): the study of the modification of chemical shifts upon complex formation for instance also provides information about the regions of interaction. Measurements of residual dipolar couplings (RDCs) provide information about the mutual orientation of partners within the complex to which they are extremely sensitive, while SAXS, that is very sensitive to translations, is little or even altogether insensitive to mutual rotations of isometric subunits [61], as beautifully illustrated in [68].

We detail the case study, of the ternary complex YgjD-YeaZ-YjeE [69]. This complex, only formed in the presence of ATP, performs a tRNA post-transcriptional modification. Using the SEC-SAXS setup on the SWING beamline and

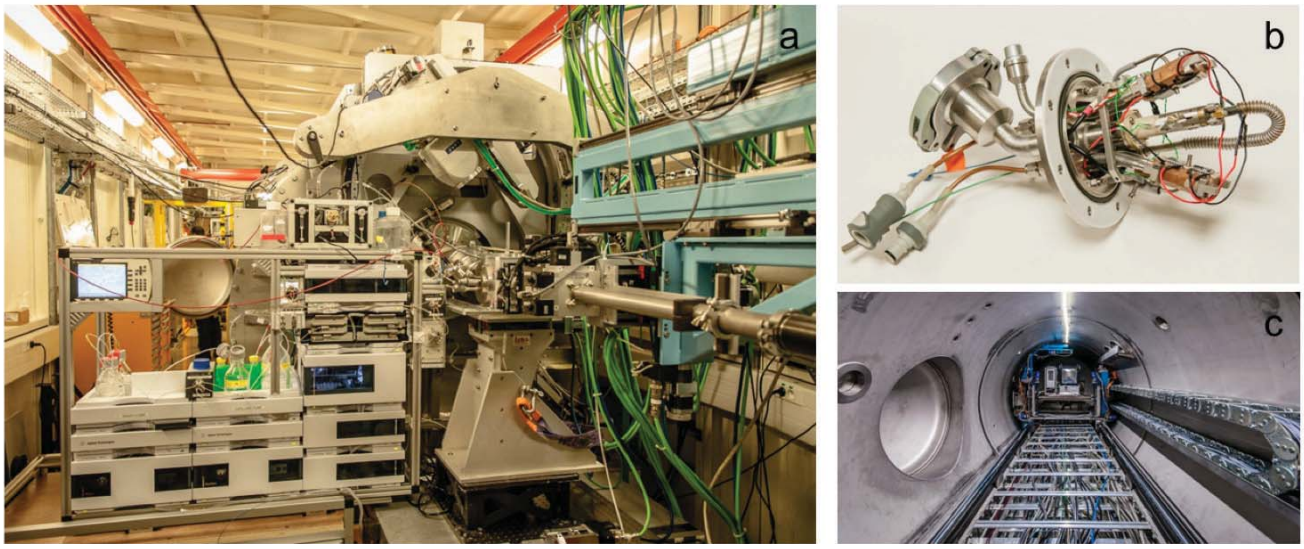

Figure 2. The SAXS/WAXS beamline SWING at SOLEIL Synchrotron
a: An overview of the experimental hutch at the SWING beamline. The HPLC set-up from Agilent© is connected to the in-vacuum SAXS measurement chamber. The X-ray path is entirely in vacuum from the source to the detector. Guard "scatterless" slits from Xenocs© are positioned at the end of the optical flight tube. The large chamber houses the Aviex© and the Imxpad© detectors.
b: The flow-through capillary cell holder, as seen from the incoming beam. The temperature is maintained to within ± 0.1 degree by Peltier elements, themselves cooled with a circulating fluid. This recent design eliminates leaks and decreases the time needed to change the capillary to less than 10 minutes.
c: Inside the detector chamber, the SAXS detectors can be translated in the three directions to adapt the q-range to the users' needs. Typically, users can switch between different detector positions within a few minutes. Several beam-stops, some of them including a Pin-diode to measure the transmitted flux, can be inserted using independent motorized stages.

adding ATP to the elution buffer, a stable complex was formed and its scattering pattern recorded. This was complemented by the study of the isolated partners. A structural model of YjeE was built using the program Phyre2 [70] from the known crystal structure of its homolog YjeE from *H. influenza* that has been solved bound to ADP. The other two partners Yeaz and YgjD form a stable binary complex whose crystal structure is known with an ADP molecule in the Yeaz-YgjD interface region. Analysis of the scattering curves of YjeE and of the YeaZ-YgjD complex allowed the authors to validate both conformations in solution. The P(r) profile of the ternary complex indicated that the maximal extension was equal to that of the binary YeaZ- YgjD complex. The dimensionless Kratky plot showed that the complex was compact, as confirmed by the envelope obtained using GASBOR (Figure **3**). Taking into account the results of biochemical studies a model of the ternary YgjD–YeaZ–YjeE complex was constructed using the program SASREF. Importantly, this model was found to exhibit a crevice large enough to accommodate the tRNA substrate.

In the case of protein/nucleic acid complexes, an additional level of complexity is associated with the different chemical nature, and therefore the different electron density, of each moiety. If available, neutron scattering can complement X-ray scattering by using the contrast variation approach in which varying the D_2O/H_2O ratio in the solvent varies the scattering contribution from each component. Careful adjustment of the contrast leaves essentially one visible component by matching the average scattering contrast of the other one [71,72]. The multi-phase *ab initio* modelling program MONSA can handle the different density contrasts and yield meaningful models [59]. This is illustrated by a recent study of the complex between the histone demethylase LSD1-CoREST1 and nucleosome (NCP) [73]. SAXS patterns of the isolated NCP and demethylase have been recorded together with the pattern of the complex. The nucleosome is a complex case since it comprises a protein and a DNA phase that cannot be treated as a unique, homogeneous phase. To overcome this difficulty, and since it is obviously impossible to obtain experimentally the DNA contribution to the SAXS pattern of nucleosome, both scattering patterns of the DNA and histone moieties were calculated. The MONSA program was run using three phases, the histone octamer, DNA, and LSD1-CoREST1. The target functions were the three experimental curves (NCP, the LSD1-CoREST1 and the native complex) and the two calculated patterns of DNA and histone core. As for all *ab initio* modeling approaches, no unique solution was obtained. Envelope models were selected that both retrieved a plausible nucleosome conformation with a satisfactory shape of the DNA and yielded a good agreement between the calculated and experimental curves (χ^2 values very close to 1 for all fits). This is exemplified by the envelope shown in Figure **3**, panel B1, that was calculated from the scattering curve shown in Figure **3**, panel B2. A generally shared feature was that LSD1-CoREST1 was seen to be interacting with DNA at one of its extremities whereas the main body of the enzyme was lying fairly close to the nucleosome. Further work using better defined, covalent complexes were analyzed taking into account the crystal structures of both partners and biochemical information that characterized the interface between the interacting domain of the demethylase, located at the end of

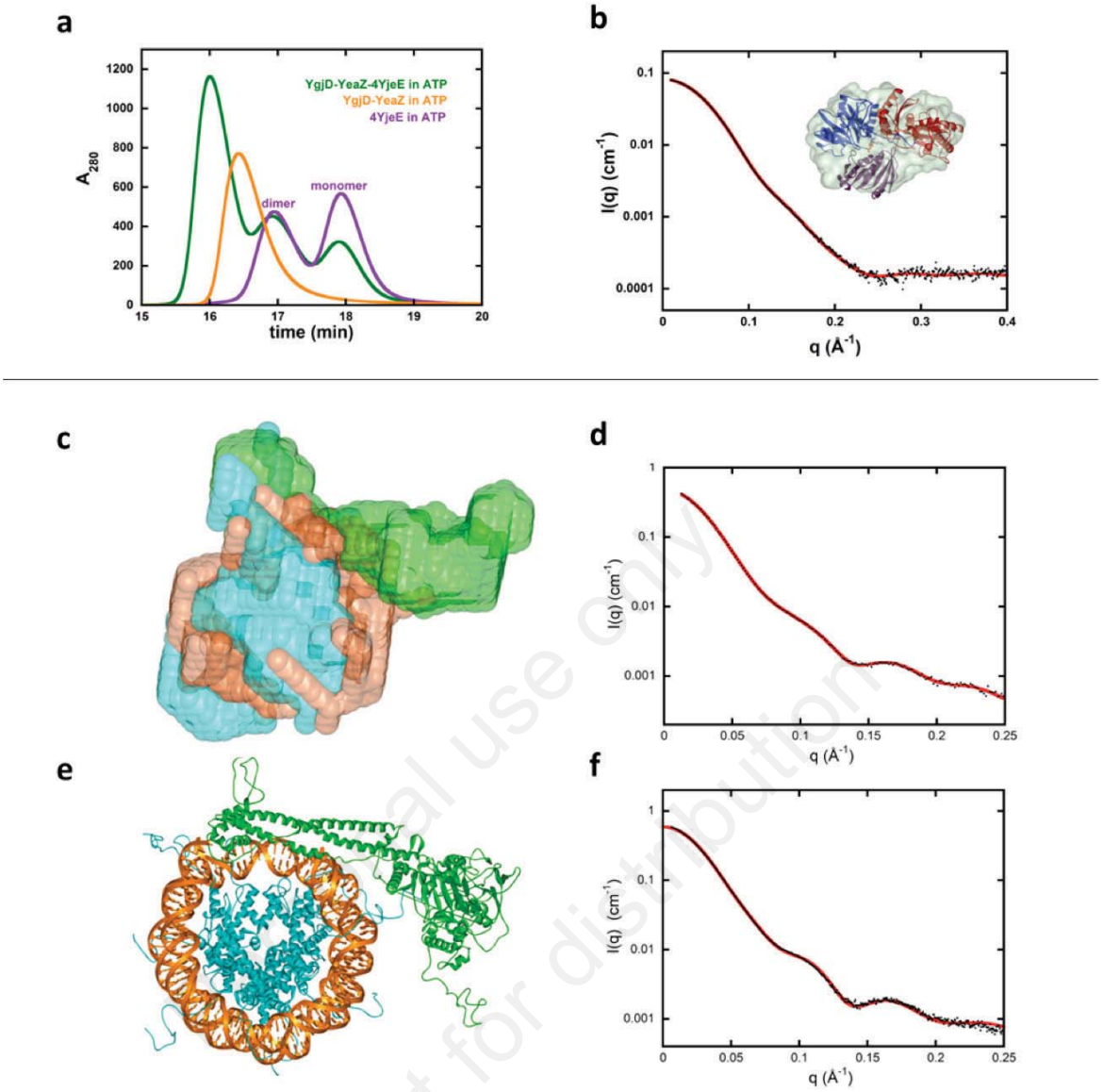

Figure 3. Two examples of complexes modeling

a: Superposition of the gel filtration profiles of YgjD–YeaZ–YjeE (green), YgjD–YeaZ (orange) and YjeE (purple) (4(E):1(DZ) molar ratio) in presence of 1.0 mM ATP and 2.0 mM $MgCl^2$.

b: Experimental SAXS scattering curve (black dots) of the YgjD–YeaZ–YjeE complex. The red line is the calculated scattering curve for the model constructed using the SASREF program. The insert presents the resulting structural model embedded in the most typical envelope extracted from the SAXS curve using the ab initio program GASBOR.

c: Interpretation of the SAXS experiments on the non-covalent LSD1-CoREST1/nucleosome 1:1 complex using the program MONSA. The envelope is shown with LSD1-CoREST1 depicted in green, the nucleosomal DNA in orange, and the histone octamer in cyan.

d: Calculated scattering curve of the MONSA model using the program CRYSOL (red line) superimposed onto the experimental scattering intensity curve of the complex (black dots).

e: All-atom model of the covalent complex. Same color code as in panel B1.

f: Calculated scattering curve of the all-atom model (red line) superimposed onto the experimental curve of the complex (black dots).

the long helical arm, and the DNA moiety. The final model shown in Figure **3**, panel B3, bears clear similarity to the MONSA model.

5. MEMBRANE PROTEINS

Membrane proteins are notoriously difficult to tackle. Despite a continuous increase, the number of known structures of membrane proteins (monitored at http://blanco.biomol.uci.edu/Membrane_Proteins_xtal.html) remains less than 2% of the total number of known protein structures, while their occurrence in the genome is about 30%. Not only is it difficult to overexpress, extract and purify them, but because they must be maintained in an amphiphilic environment, membrane proteins can never be

studied in isolation. Most frequently, membrane proteins are extracted and maintained folded in detergent solutions in which they are surrounded by a corona of detergent molecules that hides their hydrophobic surface from water. The solutions also contain micelles of pure detergent, which are spontaneously formed when the detergent concentration is above the critical micellar concentration, a pre-requisite for membrane protein solubilization [74]. The resulting coexistence of different particles in the sample and intrinsic density inhomogeneity of the protein-detergent complex requires specific strategies to analyze membrane protein structures in solution.

The most obvious strategy is to turn to Small Angle Neutron Scattering (SANS), a sister technique of SAXS, where neutrons are used instead of photons. Neutrons are scattered by the atomic nuclei instead of the electrons, and the atomic scattering lengths depend in a non-systematic way on the nature of the nuclei. The most interesting output for biological samples is that the scattering lengths of H_2O and D_2O have opposite signs, while those of biological macromolecules, proteins, nucleic acids, carbohydrates, lipids, have (different) intermediate values. It is therefore possible to cancel the average scattering contrast of one of the partners in a multi-component complex by carefully adjusting the ratio between H_2O and D_2O in the buffer. This strategy is called Contrast Matching. Applied to membrane proteins in detergent solutions, it results, in principle, in making the detergents invisible, both those from the complex corona and from the free micelles, the solution therefore appearing as a standard monodispersed protein solution, to which standard data analysis can be applied. Several studies have followed this path in the past decade, but were limited by the fact that the scattering lengths from the polar heads and from the hydrophobic tails cannot be perfectly matched simultaneously for usual detergents [75]. It recently became clearer that the resulting residual contributions of detergent corona to the scattering curve, even if small, are in fact not negligible when precise models have to be derived [75]. Accordingly, investigations in the SANS community are focusing on designing specific detergents with the highest possible scattering length homogeneity, often based on fluorinated tails [76]. In the SANS study about FhuA-pb5 complex, an individual structure within a membrane protein complex could even be described using both specific deuteration of one of the partners and a carefully designed fluorinated detergent F6-DigluM [75].

While there is no practical possibility to perform contrast matching with SAXS, the combination with SEC allows time separation between the membrane protein detergent complex and the excess of free micelles in the originally loaded sample. It also allows accurate recording of the free micelles contribution present in the elution buffer. In turn, the scattering intensity of the complex alone directly results from the subtraction of two precise experimental patterns. This opportunity was taken on the SWING beamline and allowed Berthaud *et al*. [77] to propose an accurate geometrical model of the corona of dodecyl-maltoside (DDM), the non-ionic detergent most frequently used in membrane protein biochemistry, around Aquaporin-0, a protein of known structure. The objective of this study was not uniquely to contribute to a better understanding of the physico-chemical interactions between the detergent and the hydrophobic surface of the protein, but rather to provide a precise structural starting point for further investigations of conformational changes or interactions with partners [14,77]. Unlike with contrast matching SANS measurements, there is no possibility with SAXS to directly use ab initio procedures on the full complex, which therefore prevents the easy study of unknown structures. Still, the strategy of using SEC-SAXS starting with known structures, and proceeding with unknown structural changes may also pay off, since the precision of SAXS measurements is considerably higher than that of SANS measurements. This is due partly to the much higher flux (several orders of magnitude) available at 3rd generation synchrotrons than at the most powerful neutron sources, and partly to the existence of a strong contribution of incoherent scattering in SANS. Modeling the detergent moiety has recently been facilitated by the release of the program Memprot that models a detergent corona, shaped as an elliptical torus, around a membrane protein construct of known structure [78]. A similar approach was adopted by Kaspersen *et al*. [79] to model the DDM corona around the outer-membrane protein A (OmpA), the protein being isolated as a monomer or as a dimer. Interestingly, in their study, the contribution of free micelles was evaluated as a parameter computed from data very accurately collected in absolute units, instead of being experimentally subtracted.

In parallel, the team of L. Arleth has undertaken a very ambitious research program aiming at studying low resolution structures and conformational changes of membrane proteins embedded into lipidic nanodiscs, a more physiological-like environment than detergent micelles. A precise structural determination of nanodiscs [80] or assimilated platforms [79] was undertaken using SAXS. The inclined orientation that bacteriorhodopsin adopts within a nanodisc [81], was determined mostly using SAXS, and through a careful check of the number of free parameters allowed by the experimental data using a Bayesian Indirect Fourier Transform approach [82]. More recently, using physiological lipids specifically deuterated via a biosynthetic pathway, they managed to produce a nanodisc with a neutron scattering length almost entirely matched with a buffer at 100% D2O, which is estimated to be negligible when carrying membrane proteins with a mass higher than 50 kDa [83].

6. FLEXIBLE AND INTRINSICALLY DISORDERED PROTEINS (IDP) PROTEINS

The application of SAXS to the study of these proteins has been reviewed in Receveur-Brechot and Durand [17] and in Kikhney and Svergun [84]. The expressions "flexible protein" and IDP actually designate a great variety of proteins since they comprise all proteins that do not adopt a unique, well-defined three-dimensional structure that can be determined by conventional high resolution approach, in particular by X-ray crystallography. The domain of flexible proteins and IDPs extends from totally unstructured proteins similar to polymers in good solvent and functioning as such (this is the case of small, proline-rich salivary proteins for instance) to proteins that fold upon ligand binding and to proteins mainly comprising well-structured domains together with a few less structured regions endowing the protein with a certain level of flexibility.

Before describing the various stages of SAXS data analysis that will give structural information on these proteins, we wish to specify two important points: First, we consider here interdomain flexibility, not side-chain flexibility or local flexibility within a short surface loop that SAXS, a low-resolution technique, will hardly be sensitive to. Second, by nature these proteins may theoretically adopt a great variety of conformations. It is therefore of special importance to complement SAXS by other experimental or computational approaches so as to constrain the solution space of conformations by additional information. The complementary technique of choice - and actually among the most widely used - is NMR (for a global view read for instance [85-88]) FRET must also be mentioned (a good example can be found in Gruszka *et al*., 2015 [89]) as well as hydrogen/deuterium exchange analyzed by mass spectrometry [90] and molecular dynamics calculations (see e.g. Zhang *et al*., 2015). More generally, each biochemical, biophysical or computational technique that yields a structural constraint is useful and is worth considering. Even more than in the case of well-structured objects « synergistic use of complementary information and hybrid modelling are the most promising ways »[1].

Three successive stages can be distinguished in SAXS data analysis [91]. We first start with a qualitative examination of the SAXS patterns. According to P. Bernado [92], "features of SAXS data that identify flexible proteins are: (1) general attenuation of fine structure in the scattering profiles, which becomes more dramatic in Kratky representations, and (2) a reduced number of interdomain correlation peaks in p(r) functions that also present large D_{max} values and a smooth decrease to 0." This does not lead to unambiguous conclusions but can only raise a suspicion of flexibility. One should also examine the data using the already mentioned dimensionless Kratky plot - $(qR_g)^2I(q)/I(0)$ *vs* qR_g - that emphasizes the non-globularity of the object. A horizontal plateau or a linear increase observed at larger angle strongly suggests a marked flexibility but may also reflect a strong anisometry. If one remembers Porod's law and associated plot $q^4I(q)$ *vs* q - a particle of uniform density and sharp interface with the surrounding medium exhibits a q^{-4} asymptotic behaviour - , the absence of an approximate plateau in a Porod plot may reflect the absence of a well-defined interface, as is the case in a flexible unstructured protein [93], or again a strong anisometry. In fact, these qualitative features can only be interpreted in the framework of all other information about the protein under study such as clear evidence for disordered regions resulting from amino-acid sequence analysis by disorder predictors.

The second stage corresponds to the case where large disordered regions are revealed by sequence analysis and when the protein is known not to possess large, well-structured domains. Here, one may apply polymer theory and describe the scattering pattern using analytical mathematical models. One can start by comparing the experimentally determined value of the radius of gyration to that obtained from scaling laws [17]: $R_g=R_0N^{\nu}$, where N is the residue number while R_0 and ν depend on the level of residual structure of the scattering object. Bernado and Blackledge [94] report values of R_0=2.54 and ν =0.522 for IDPs. This is very limited information, all the more so that R_g determination is not always easy for a large size, extended flexible protein since the Guinier range, restricted to very small angles, is often not experimentally accessible. More appropriate is the attempt to describe all (or a significant part of) the scattering pattern using an analytical expression. In the case of a protein deprived of any large structured domains and exhibiting nothing more than local structure, the appropriate expression, proposed by Sharp and Bloomfield for a chain with persistence length [17] depends on three structural parameters that are determined in the fit against the data: the contour length of the chain *L*, the size *b* of the constitutive statistical elements and the radius of gyration of its cross-section R_c [22]. These parameter values give indications on the rigidity of the polypeptide chain and on the possible existence of secondary structure elements. A second type of function has been developed by Capp *et al*. [91] to describe the case of proteins comprising well-structured domains with intervening flexible linkers in a pearl necklace-like arrangement.

The last stage aims at a description of the protein using an ensemble of atomic models rather than a unique model, which is meaningful in view of the large conformational space explored by the protein. This kind of approach was pioneered by Bernado *et al*. (Ensemble Optimization Method, EOM, 2007) recently upgraded in Tria *et al.* [95]. In the following years, other groups developed similar approaches, such as Minimal Ensemble Search, MES [30], Basis-Set Supported SAXS, BSS-SAXS [96], Ensemble Refinement Of SAXS, EROS [97] and maximum occurrence method, MaxOcc [98]. The common strategy to all these approaches is to create a very large library of conformations before selecting, within this library, ensembles of conformations whose average scattering curve fits the experimental curve. Information about the solution space is directly obtained from the comparison between the distributions of global structural parameters such as R_g or D_{max} corresponding to the optimized ensembles and the total pool respectively. Beyond this straightforward comparison (identical distributions or distribution of the optimized ensemble shifted towards small (large) values), features such as a bimodal distribution suggesting the coexistence of compact and extended conformations in solution should be validated by other experimental approaches such as AFM [99,100] but also NMR. The incorporation of NOEs and RDCs in the refinement protocol improves both the construction of the pool and the determination of fitting ensembles [88]. The determination of ensembles is particularly robust in the case of the EROS method that uses a maximum entropy protocol to fit the experimental scattering data as beautifully illustrated in Köfinger *et al*. [101].

7. KINETIC STUDIES

Since the very beginning of the use of SR for SAXS measurements, time-resolved experiments have been at the cutting edge in the field. They are still not very common compared with the numerous applications of more conventional, "static" experiments. This is due to the severe requirements in terms of instrumental development, sample amount and to the relatively small number of well-suited systems. However, the availability of high quality, very in-

[1] D. Svergun, EMBO lecture, 2012

tense X-ray micro-beams at 3rd and 4th generation sources sparked a regain of interest in these studies. The approach uses a fast perturbation of the system out of equilibrium and the relaxation of the system is monitored by SAXS. Classically, perturbation is triggered by fast-mixing with the perturbing agent. Stopped-flow instruments have been used for decades and provide mixing times down to the ms range. Faster mixing is obtained using continuous flow setups in which the time resolution is obtained by adjusting the distance between the irradiated volume and the mixing point. Coupled with micro-fluidic devices and the availability of micro-beams that allow a considerable reduction in sample volume requirement, this approach seems now promised to a very bright future. Perturbation is also triggered by using a photoactivatable compound that, upon laser illumination, releases the perturbing agent. Here, time resolution is essentially limited by the X-ray pulse width that is typically a fraction of a ns at storage rings and a fraction of a ps at free-electron lasers. These very fast processes are monitored not strictly speaking by SAXS but at large angles (WAXS) and accumulation of repeated changes using a very intense beam [102,103].

Three main types of processes have been investigated using TR-SAXS: assembly, macromolecule (un)folding and conformational changes. Several self-assembling systems will be presented in the next section. Macromolecules also assemble and the formation of viral capsid from coat protein solutions upon acidification and of full viral particle upon coat protein and RNA interaction are excellent examples [104]. Another case in point is the very complex and dynamic process of micro-tubule association and dissociation. Object of a seminal study by Mandelkow and Bordas in the 80s' [105], this process is currently revisited using much improved data, analysis software and the available tubulin crystal structures. Fibrin assembly following fibrinogen activation has been recently investigated in a multi-scale study coupling TR-SAXS and TR-MALS (multi-angle light scattering) [106]. The elongation of the protofibrils was monitored by MALS while X-ray scattering patterns probed the time evolution of the fibril thickness. The unprecedented combination of both techniques allowed the authors to rule out the classical model of half-staggered, double-stranded fibrils and led to the proposal of a modified model accounting for both experimental data sets together with a variety of other observations. Protein folding was also a major topic of TR studies from the early days. A landmark study is that of apomyoglobin refolding upon pH increase using continuous flow mixing TR-SAXS coupled with other spectroscopic kinetic studies [107]. Several proteins were subsequently investigated by this multi-technique approach that led to some global insights into the major determinants of tertiary structure and of the folding process. RNA folding was also studied in a parallel effort led mainly by two groups in the United States and reviewed in [108]. Finally conformational transitions were studied in allosteric enzyme ATCase from E. coli [109] and for viral particles [110,111] with a time-resolution ranging from the s down to the ms range while much faster processes in hemoglobin [103] and photosynthetic reaction center [102] were investigated in the WAXS regime. Without entering into any specific detail of TR-data analysis, a very commonly used tool since the early days of TR-SAXS [112,113] deserves a special mention: the Singular Value Decomposition (SVD) analysis, that allows one to detect the existence of intermediate(s) in a structural transition, a prerequisite to the design of any molecular mechanism.

Beyond the special case of FEL radiation the perspectives with more conventional SR point towards a dramatic reduction in the necessary sample volume through the use of micro-beam with microfluidic mixers. The disappearance of this very severe bottleneck might lead to an extension of TR-SAXS application to a greater variety of biological systems. The other direction is that of multi-scale studies that combine various probes on the same sample to study the structural dynamics of processes involving the elongation and thickening of fibrous-like structures (e.g., collagen, β-amyloid). Here, speed is not of the essence, but rather the ability to monitor over the largest possible range of dimensions various features of the supramolecular assemblies, thereby offering a more complete view of the process.

8. LARGE SUPRAMOLECULAR ASSEMBLIES

Solutions are not the only state where SAXS can bring information about peptides or proteins. Assembled materials made of proteins or peptides can also largely benefit from SAXS measurements. When isolated macromolecules assemble into regular structures, new correlations appear in the electronic density of the whole structure, giving rise to specific modulations in the scattering intensity. When motifs are repeated along a defined axis with a repetition distance d, the scattered photon waves undergo strong constructive interferences at q values given by the relation $q = n\frac{2\pi}{d}$, where n is an integer (Bragg law). The phenomenon is called diffraction, but is not different in nature from solution scattering. When identical units, *e.g.* a peptide or a protein, are regularly spaced, with periodicities typically of the order of or larger than 1 nm, diffraction is observed in the Small Angle range [114] (SAXD). In this chapter we focus on self-assembled samples. Self-assembly is a process in which randomly arranged components form an organized structure as a consequence of intrinsic interactions without external stimuli. For peptides or proteins, two mains families of self-assemblies emerge: fiber growth, for which there is no control on the final object size, shape or number of primitive units and controlled self-assembled materials, for which the primitive unit precisely defines the final object due to its specific shape [115], possible interactions [116] and size [117,118].

Using synchrotron radiation for these studies is an absolute requirement due to the large number of samples needed to understand mechanisms of the self-assembly process, intermediary structures and final structures.

8.1. Fiber Growth

One of the main goals of studying non-controlled peptide assemblies is to understand the formation of amyloid fibrils or amyloid-like fibrils (Figure **4a**). Indeed such materials are responsible for, or at least correlated with, a wide range of diseases such as Alzheimer, diabetes type 2 and Parkinson's disease [119]. SAXS synchrotron beamlines are the right tool

to determine amyloids and amyloid-like structures by dint of high photon flux and high quality setups. A number of groups such as Eisenberg's group at UCLA or Gazit's group at Tel Aviv University have been working on understanding amyloid structure and formation (Figure **4a**) [120-124]. These studies established that amyloid fibrils were formed of β-strand peptide sequences arranged in a specific manner.

Thus amyloid fibril formation and final structures are now well known. Based on amyloid or amyloid-like fibril properties [123,124], research is presently focusing on the use of fibrils as backbones for functional materials [123,124, 126-128]. Modified fibers serve in the formation of hollow nanotubes that can be used as templates for the fabrication of nanowires. First, metallic ions are let to diffuse in the fiber lumen before enzymatic degradation of the fiber scaffold results in the production of nanoscale wires. Another possibility is the deposition of metal on the fiber surface which would result in a coaxial nano-cable [125]. Those fibrils can assemble to form conducting nanowires, or can be used as surface coating and nanostructured protein film [124].

The structures of modified or functionalized fibrils are analyzed by SAXS to confirm that the amyloid structure is not altered while their function is checked using other methods (Figure **4b**). SAXD hence allows fiber structural characterization, starting from its formation, its structure before and after modification up to the final object. Moreover, using synchrotron radiation facilitates the access to other complementary techniques such as circular dichroism (SRCD) [129], also available at some facilities, which provide valuable information with an extended wavelength range about the peptide secondary structure, especially for dilutes samples.

8.2. Controlled Self-Assemblies

Proteins can act as scaffolds for cellular structural stability. This implies the control of the scaffold assembly by protein/peptide interactions. Learning from these interactions, mostly arising from non-covalent binding, it is possible to create short peptide structures for which control towards a designed final object is possible [130,131]. A well-known example of controlled self-assembly is the self-assembly of peptides nanotubes. There are several classes of peptides that can form nanotubes, cyclic peptides [132], surfactant like peptides [133], amyloid peptides [134].

Here we briefly discuss cyclic peptides nanotubes, for which the final structure can be fixed by modifying the peptide residue, the nature of counter ions or the buffer properties (pH, salts and composition). Some of them have direct industrial applications [135-138]. One of these peptides, an octapeptide called Lanreotide, is used as a growth inhibitor

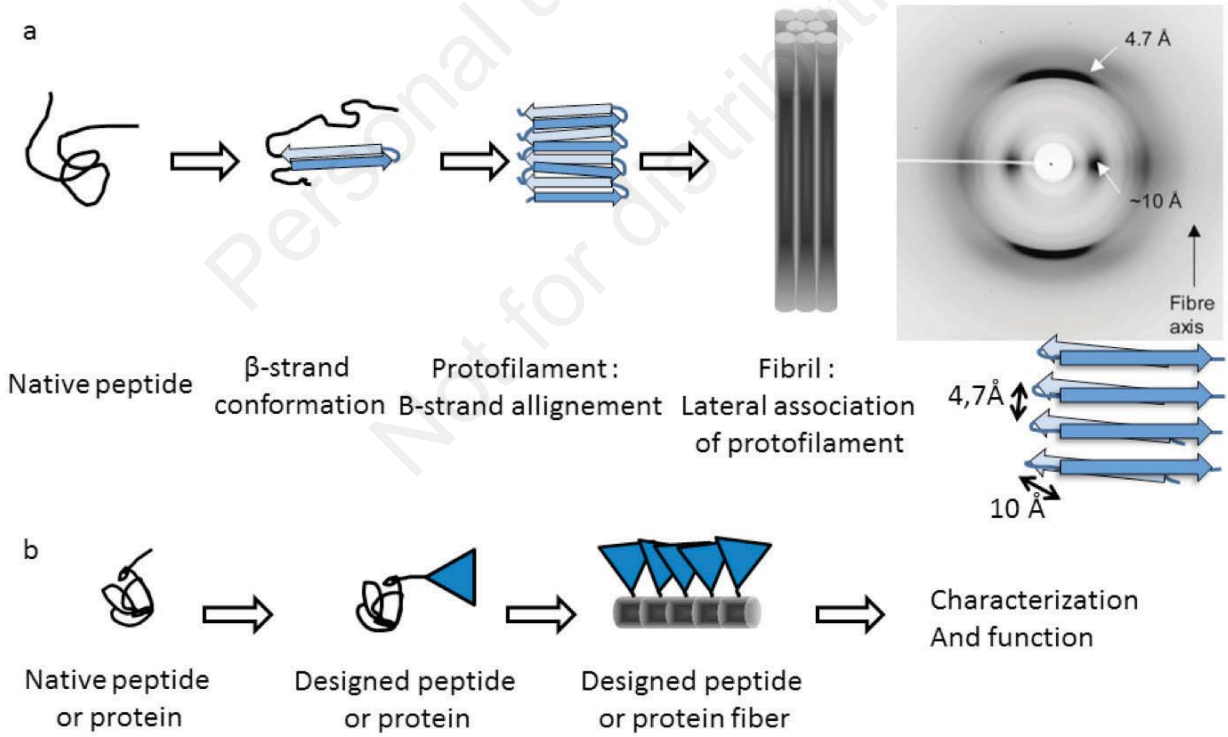

Figure 4. Self-assembling systems

a/ Amyloids hierarchical formation sketch. Peptides or protein unfold and acquire a β-strand secondary structure. These β-strands then assemble into protofibrils. The β-strands are perpendicular to the protofibrils main axis. The protofibrils then assemble into fibrils by lateral association. The experimental image shows a typical amyloid fiber diffraction pattern. The anisotropic reflections are indicative of a partially aligned fiber, perpendicular to the X-ray beam. The reflections at d=4.7Å and d=10 Å correspond respectively to the inter-β-strand and inter-β-sheet spacing.

b/ Conjugation of amyloidogenic motifs and functional proteins which form functional fibers that retain the proteins activity [125]. The aim is to modify the natural peptide functional side chain in order to add a specific function to the fiber. SAXD is widely used to find the fiber structure before and after modification.

hormone; it can display a very large variety of hollow nanotube structures simply by changing the counter ion, or by chemically modifying a lateral chain. These two parameters mainly affect the nanotube diameter through two different mechanisms. First, SAXS studies showed that the counterions have a steric effect in areas where close contacts occur and can tune the nanotube diameter. So increasing the steric hindrance of the counter ion will increase the nanotube diameter and conversely [137]. Finally, the lysine side chain of the octapeptide, which is involved in a steric close contact, can be modified in length or steric hindrance. This modification of the peptide sequence induces a diameter change, which is inversely proportional to the length/steric hindrance of the new peptide residue. Crystallization of the peptide nanotube was achieved using L-1,3-diamino propionic acid instead of lysine. The X-ray diffraction pattern from the crystalline powder of the modified octapeptide combined with Wide-Angle X-ray Scattering (WAXS, which probes very small distances on the same sample) allowed the 3D reconstruction of the crystal lattice and hence of the fundamental unit [138].

9. CONCLUSION

BioSAXS has become a mature technique over the last decade. Intense theoretical research is currently conducted in several groups worldwide to improve the reliability of the data interpretation. Many new SAXS beamlines developments at several synchrotron facilities are driven by BioSAXS requirements. The technique is now clearly an indispensable tool in Structural Biology, as a complement to high-resolution techniques. We have attempted here to provide the reader with a flavor of the ever growing possibilities offered by BioSAXS in Structural Biology, together with a simple description of the tools currently developed. The perspectives in mainstream SAXS are focused around sample volume reduction, automation of data acquisition, reduction and analysis procedures. Several directions are still at an exploratory stage: use of deep-frozen samples [139], lab-on–a–chip for systematic variations of experimental conditions, use of coherence at FEL facilities [140,141], that may give rise to new applications of scattering by biological macromolecules.

CONFLICT OF INTEREST

The authors confirm that this article content has no conflict of interest.

ACKNOWLEDGEMENTS

We are grateful to Claude Menneglier for his pictures of the SWING beamline.

REFERENCES

[1] Guinier, A. *Small-angle scattering of x-rays*. Structure of matter series, Wiley [u.a.], **1955**.

[2] Glatter, O.; Kratky, O. *Small angle x-ray scattering / edited by O. Glatter and O. Kratky*, London ; New York : Academic Press, **1982**.

[3] Feigin, L.A.; Svergun, D.I.; Taylor, G.W. *Structure analysis by small-angle X-ray and neutron scattering* (Taylor, G. W., Ed.), Plenum, Place of Publication: New York, NY, USA. Country of Publication: USA, **1987**.

[4] Svergun, D.; Barberato, C.; Koch, M.H.J. CRYSOL-a program to evaluate X-ray solution scattering of biological macromolecules from atomic coordinates. *J. Appl. Crystallogr.*, **1995**, *28*, 768-773.

[5] Koch, M.H.J.; Vachette, P. Solution X-ray scattering on biological samples. *Synchrotron Rad. News*., **1989**, *2*, 16.

[6] Rambo, R.P.; Tainer, J.A. Bridging the solution divide: comprehensive structural analyses of dynamic RNA, DNA, and protein assemblies by small-angle X-ray scattering. *Curr. Opin. Struct. Biol*., **2010**, *20*, 128-37.

[7] Perez, J.; Nishino, Y. Advances in X-ray scattering: from solution SAXS to achievements with coherent beams. *Curr. Opin. Struct. Biol*., **2012**, *22*, 670-8.

[8] Graewert, M.A.; Svergun, D.I. Impact and progress in small and wide angle X-ray scattering (SAXS and WAXS). *Curr. Opin. Struct. Biol*., **2013**, *23*, 748-54.

[9] Kirby, N.M.; Cowieson, N.P. Time-resolved studies of dynamic biomolecules using small angle X-ray scattering. *Curr. Opin. Struct. Biol*., **2014**, *28*, 41-6.

[10] Fang, X.; Stagno, J.R.; Bhandari, Y.R.; Zuo, X.; Wang, Y.X. Small-angle X-ray scattering: a bridge between RNA secondary structures and three-dimensional topological structures. *Curr. Opin. Struct. Biol*., **2015**, *30*, 147-60.

[11] Svergun, D.I.; Koch, M.H.J.; Timmins, P.A.; May, R.P. *Small Angle X-Ray and Neutron Scattering from Solutions of Biological Macromolecules*, Oxford University Press, **2013**.

[12] Jacques, D.A.; Guss, J.M.; Trewhella, J. Reliable structural interpretation of small-angle scattering data from bio-molecules in solution--the importance of quality control and a standard reporting framework. *BMC Struct. Biol*., **2012**, *12*, 9.

[13] Koch, M.H.; Vachette, P.; Svergun, D.I. Small-angle scattering: a view on the properties, structures and structural changes of biological macromolecules in solution. *Q Rev. Biophys*., **2003**, *36*, 147-227.

[14] Koutsioubas, A.; Berthaud, A.; Mangenot, S.; Perez, J. Ab initio and all-atom modeling of detergent organization around Aquaporin-0 based on SAXS data. *J. Phys. Chem. B*.; **2013**, *117*, 13588-94.

[15] Doniach, S.; Lipfert, J. 1.18 Small and Wide Angle X-ray Scattering from Biological Macromolecules and their Complexes in Solution. *Compr. Biophys*., **2012**, 376-397.

[16] Durand, D.; Vives, C.; Cannella, D.; Perez, J.; Pebay-Peyroula, E.; Vachette, P.; Fieschi, F. NADPH oxidase activator p67(phox) behaves in solution as a multidomain protein with semi-flexible linkers. *J. Struct. Biol*., **2010**, *169*, 45-53.

[17] Receveur-Brechot, V.; Durand, D. How random are intrinsically disordered proteins? A small angle scattering perspective. *Curr. Protein Pept. Sci*., **2012**, *13*, 55-75.

[18] Roblin, P.; Potocki-Veronese, G.; Guieysse, D.; Guerin, F.; Axelos, M.A.V.; Perez, J.; Buleon, A. SAXS Conformational Tracking of Amylose Synthesized by Amylosucrases. *Biomacromolecules*, **2013**, *14*, 232-239.

[19] Oda, T.; Iwasa, M.; Aihara, T.; Maeda, Y.; Narita, A. The nature of the globular-to fibrous-actin transition (English). *Nature (Lond.)*, **2009**, *457*, 441-445.

[20] Graille, M.; Cladière, L.; Durand, D.; Lecointe, F.; Gadelle, D.; Quevillon-Cheruel, S.; Vachette, P.; Forterre, P.; van Tilbeurgh, H. Article: Crystal Structure of an Intact Type II DNA Topoisomerase: Insights into DNA Transfer Mechanisms. *Structure*, **2008**, *16*, 360-370.

[21] Durand, D.; Vives, C.; Cannella, D.; Perez, J.; Pebay-Peyroula, E.; Vachette, P.; Fieschi, F. NADPH oxidase activator p67(phox) behaves in solution as a multidomain protein with semi-flexible linkers. *J. Struct. Biol*., **2010**, *169*, 45-53.

[22] Boze, H.; Marlin, T.; Durand, D.; Perez, J.; Vernhet, A.; Canon, F.; Sarni-Manchado, P.; Cheynier, V.; Cabane, B. Proline-rich salivary proteins have extended conformations. *Biophys. J.*, **2010**, *99*, 656-65.

[23] Svergun, D.I. Determination of the Regularization Parameter in Indirect -Transform Methods Using Perceptual Criteria. *J. Appl. Cryst*., **1992**, *25*, 495-503.

[24] Schneidman-Duhovny, D.; Hammel, M.; Sali, A. FoXS: a web server for rapid computation and fitting of SAXS profiles. *Nucleic Acids Res*., **2010**, *38*, W540-4.

[25] Chen, P.C.; Hub, J.S. Validating solution ensembles from molecular dynamics simulation by wide-angle X-ray scattering data. *Biophys J*., **2014**, *107*, 435-47.

[26] Petoukhov, M.V.; Svergun, D.I. Global rigid body modeling of macromolecular complexes against small-angle scattering data. *Biophys J*., **2005**, *89*, 1237-50.

[27] Petoukhov, M.V.; Franke, D.; Shkumatov, A.V.; Tria, G.; Kikhney, A.G.; Gajda, M.; Gorba, C.; Mertens, H.D.T.; Konarev, P.V.; Svergun, D.I. New developments in the ATSAS program package for small-angle scattering data analysis. *J. Appl. Crystallogr*., **2012**, *45*, 342-350.

[28] Moore, B.L.; Kelley, L.A.; Barber, J.; Murray, J.W.; MacDonald, J.T. High-quality protein backbone reconstruction from alpha carbons using Gaussian mixture models. *J. Comput. Chem*., **2013**, *34*, 1881-9.

[29] Weinkam, P.; Pons, J.; Sali, A. Structure-based model of allostery predicts coupling between distant sites. *Proc. Natl. Acad. Sci. USA*, **2012**, *109*, 4875-80.

[30] Pelikan, M.; Hura, G.L.; Hammel, M. Structure and flexibility within proteins as identified through small angle X-ray scattering. *Gen. Physiol. Biophys*., **2009**, *28*, 174-89.

[31] Evrard, G.; Mareuil, F.; Bontems, F.; Sizun, C.; Perez, J. DADIMODO: a program for refining the structure of multidomain proteins and complexes against small-angle scattering data and NMR-derived restraints. *J. Appl. Crystallogr*., **2011**, *44*, 1264-1271.

[32] Curtis, J.E.; Raghunandan, S.; Nanda, H.; Krueger, S. SASSIE: A program to study intrinsically disordered biological molecules and macromolecular ensembles using experimental scattering restraints. *Compu. Phys. Commun*., **2012**, *183*, 382-389.

[33] Schwieters, C.D.; Clore, G.M. Using small angle solution scattering data in Xplor-NIH structure calculations. *Prog. Nucl. Magn. Reson. Spectrosc.*, **2014**, *80*, 1-11.

[34] Svergun, D.I. Restoring low resolution structure of biological macromolecules from solution scattering using simulated annealing. *Biophys. J*., **1999**, *76*, 2879-86.

[35] Franke, D.; Svergun, D.I. DAMMIF, a program for rapid *ab-initio* shape determination in small-angle scattering. *J. Appl. Cryst*., **2009**, *42*, 342-346.

[36] Koutsioubas, A.; Perez, J. Incorporation of a hydration layer in the `dummy atom' ab initio structural modelling of biological macromolecules. *J. Appl. Crystallogr*., **2013**, *46*, 1884-1888.

[37] Svergun, D.I.; Petoukhov, M.V.; Koch, M.H. Determination of domain structure of proteins from X-ray solution scattering. *Biophys J*., **2001**, *80*, 2946-53.

[38] Delpierre, P.; Basolo, S.; Berar, J.-F.; Bordesoule, M.; Boudet, N.; Breugnon, P.; Caillot, B.; Chantepie, B.; Clemens, J.C.; Dinkespiler, B.; Hustache-Ottini, S.; Meessen, C.; Menouni, M.; Morel, C.; Mouget, C., Pangaud, P., Potheau, R.; Vigeolas, E. XPAD: A photons counting pixel detector for material sciences and small-animal imaging. *Nucl. Instrum. Methods Phys. Res. A*., **2007**, *572*, 250-253.

[39] Wernecke, J.; Gollwitzer, C.; Müller, P.; Krumrey, M. Characterization of an in-vacuum PILATUS 1M detector. *J. Synchrotron Rad*., **2014**, *21*, 529-536.

[40] David, G.; Pérez, J. Combined sampler robot and high-performance liquid chromatography: a fully automated system for biological small-angle X-ray scattering experiments at the Synchrotron SOLEIL SWING beamline. *J. Appl. Crystallogr*., **2009**, *42*, 892-900.

[41] Blanchet, C.E.; Spilotros, A.; Schwemmer, F.; Graewert, M.A.; Kikhney, A.; Jeffries, C.M.; Franke, D.; Mark, D.; Zengerle, R.; Cipriani, F.; Fiedler, S.; Roessle, M.; Svergun, D.I. Versatile sample environments and automation for biological solution X-ray scattering experiments at the P12 beamline (PETRA III, DESY). *J. Appl. Crystallogr*., **2015**, *48*, 431-443.

[42] Dubuisson, J.M.; Decamps, T.; Vachette, P. Improved signal-to-background ratio in small-angle X-ray scattering experiments with synchrotron radiation using an evacuated cell for solutions. *J. Appl. Crystallogr.*, **1997**, *30*(1), 49-54.

[43] Round, A.R.; Franke, D.; Moritz, S.; Huchler, R.; Fritsche, M.; Malthan, D.; Klaering, R.; Svergun, D.I.; Roessle, M. Automated sample-changing robot for solution scattering experiments at the EMBL Hamburg SAXS station X33. *J. Appl. Crystallogr*., **2008**, *41*, 913-917.

[44] Lurio, L.; Mulders, N.; Paetkau, M.; Jemian, P.R.; Narayanan, S.; Sandy, A. Windows for small-angle X-ray scattering cryostats. *J. Synchrotron* Rad., **2007**, *14*, 527-531.

[45] Kirby, N.M.; Mudie, S.T.; Hawley, A.M.; Cookson, D.J.; Mertens, H.D.T.; Cowieson, N.; Samardzic-Boban, V. A low-background-intensity focusing small-angle X-ray scattering undulator beamline. *J. Appl. Crystallogr*., **2013**, *46*, 1670-1680.

[46] Acerbo, A.S.; Cook, M.J.; Gillilan, R.E. Upgrade of MacCHESS facility for X-ray scattering of biological macromolecules in solution. *J. Synchrotron Rad*., **2015**, *22*, 180-186.

[47] Li, Y.; Beck, R.; Huang, T.; Choi, M.C.; Divinagracia, M. Scatterless hybrid metal–single-crystal slit for small-angle X-ray scattering and high-resolution X-ray diffraction. *J. Appl. Crystallogr*., **2008**, *41*, 1134-1139.

[48] Round, A.R.; Franke, D.; Moritz, S.; Huchler, R.; Fritsche, M.; Malthan, D.; Klaering, R.; Svergun, D.I.; Roessle, M. Automated sample-changing robot for solution scattering experiments at the EMBL Hamburg SAXS station X33. *J. Appl. Crystallogr.*, **2008**, *41*, 913-917.

[49] Hura, G.L.; Menon, A.L.; Hammel, M.; Rambo, R.P.; Poole, F.L.; Tsutakawa, S.E.; Jenney, F.E.; Classen, S.; Frankel, K.A.; Hopkins, R.C.; Yang, S.-J.; Scott, J.W.; Dillard, B.D.; Adams, M.W.W.; Tainer, J.A. Robust, high-throughput solution structural analyses by small angle X-ray scattering (SAXS). *Nat. Methods*, **2009**, *6*, 606-612.

[50] Martel, A.; Liu, P.; Weiss, T.M.; Niebuhr, M.; Tsuruta, H. An integrated high-throughput data acquisition system for biological solution X-ray scattering studies. *J. Synchrotron Rad*., **2012**, *19*, 431-434.

[51] Blanchet, C.E.; Spilotros, A.; Schwemmer, F.; Graewert, M.A.; Kikhney, A.; Jeffries, C.M.; Franke, D.; Mark, D.; Zengerle, R.; Cipriani, F.; Fiedler, S.; Roessle, M.; Svergun, D.I. Versatile sample environments and automation for biological solution X-ray scattering experiments at the P12 beamline (PETRA III, DESY). *J. Appl. Crystallogr*., **2015**, *48*, 431-443.

[52] Didry, D.; Cantrelle, F.X.; Husson, C.; Roblin, P.; Moorthy, A.M.; Perez, J.; Le Clainche, C.; Hertzog, M.; Guittet, E.; Carlier, M.F.; van Heijenoort, C.; Renault, L. How a single residue in individual beta-thymosin/WH2 domains controls their functions in actin assembly. *EMBO J*., **2012**, *31*, 1000-13.

[53] Brookes, E.; Pérez, J.; Cardinali, B.; Profumo, A.; Vachette, P.; Rocco, M. Fibrinogen species as resolved by HPLC-SAXS data processing within the UltraScan Solution Modeler (US-SOMO) enhanced SAS module. *J. Appl. Crystallogr*., **2013**, *46*, 1823-1833.

[54] Malaby, A.W.; Chakravarthy, S.; Irving, T.C.; Kathuria, S.V.; Bilsel, O.; Lambright, D.G. Methods for analysis of size-exclusion chromatography-small-angle X-ray scattering and reconstruction of protein scattering. *J. Appl. Crystallogr*., **2015**, *48*, 1102-1113.

[55] Graewert, M.A.; Franke, D.; Jeffries, C.M.; Blanchet, C.E.; Ruskule, D.; Kuhle, K.; Flieger, A.; Schafer, B.; Tartsch, B.; Meijers, R.; Svergun, D.I. Automated pipeline for purification, biophysical and x-ray analysis of biomacromolecular solutions. *Sci. Rep*., **2015**, *5*, 10734.

[56] Lafleur, J.P.; Snakenborg, D.; Nielsen, S.S.; Møller, M.; Toft, K.N.; Menzel, A.; Jacobsen, J.K.; Vestergaard, B.; Arleth, L. Kutter, J.P. Automated microfluidic sample-preparation platform for high-throughput structural investigation of proteins by small-angle X-ray scattering. *J. Appl. Crystallogr*., **2011**, *44*, 1090-1099.

[57] Skou, M.; Skou, S.; Jensen, T.G.; Vestergaard, B.; Gillilan, R.E. In situ microfluidic dialysis for biological small-angle X-ray scattering. *J. Appl. Crystallogr*., **2014**, *47*, 1355-1366.

[58] Martel, A.; Burghammer, M.; Davies, R.; Dicola, E.; Panine, P.; Salmon, J.-B.; Riekel, C. A microfluidic cell for studying the formation of regenerated silk by synchrotron radiation small- and wide-angle X-ray scattering. *Biomicrofluidics*, **2008**, *2*, 24104.

[59] Petoukhov, M.V.; Franke, D.; Shkumatov, A.V.; Tria, G.; Kikhney, A.G.; Gajda, M.; Gorba, C.; Mertens, H.D.T.; Konarev, P.V.; Svergun, D.I. New developments in the ATSAS program package for small-angle scattering data analysis. *J. Appl. Cryst.*, **2012**, *45*, 342-350.

[60] Schneidman-Duhovny, D., Hammel, M.; Tainer, J.A.; Sali, A. Accurate SAXS profile computation and its assessment by contrast variation experiments. *Biophys. J*., **2013**, *105*, 962-974.

[61] Mareuil, F.; Sizun, C.; Perez, J.; Schoenauer, M.; Lallemand, J.Y.; Bontems, F. A simple genetic algorithm for the optimization of multidomain protein homology models driven by NMR residual dipolar coupling and small angle X-ray scattering data. *Eur. Biophys. J*., **2007**, *37*, 95-104.

[62] De Maria Antolinos, A.; Pernot, P.; Brennich, M.E.; Kieffer, J.; Bowler, M.W.; Delageniere, S.; Ohlsson, S.; Malbet Monaco, S.; Ashton, A.; Franke, D.; Svergun, D.; McSweeney, S.; Gordon, E.; Round, A. ISPyB for BioSAXS, the gateway to user autonomy in solution scattering experiments. *Acta Crystallogr. D Biol. Crystallogr*., **2015**, *71*, 76-85.

[63] Schmitt, E.; Panvert, M.; Lazennec-Schurdevin, C.; Coureux, P.D.; Perez, J.; Thompson, A.; Mechulam, Y. Structure of the ternary initiation complex aIF2-GDPNP-methionylated initiator tRNA. *Nat. Struct. Mol. Biol*., **2012**, *19*, 450-4.

[64] Russel, D.; Lasker, K.; Webb, B.; Velazquez-Muriel, J.; Tjioe, E.; Schneidman-Duhovny, D.; Peterson, B.; Sali, A. Putting the pieces together: integrative modeling platform software for structure determination of macromolecular assemblies. *PLoS Biol*., **2012**, *10*, e1001244.

[65] Peng, Y.; Curtis, J.E.; Fang, X.; Woodson, S.A. Structural model of an mRNA in complex with the bacterial chaperone Hfq. *Proc. Natl. Acad. Sci. USA*, **2014**, *111*, 17134-9.

[66] Webb, S.; Hector, R.D.; Kudla, G.; Granneman, S. PAR-CLIP data indicate that Nrd1-Nab3-dependent transcription termination regulates expression of hundreds of protein coding genes in yeast. *Genome Biol*., **2014**, *15*, R8.

[67] Hennig, J.; Sattler, M. The dynamic duo: combining NMR and small angle scattering in structural biology. *Protein Sci*., **2014**, *23*, 669-82.

[68] Venditti, V.; Schwieters, C.D.; Grishaev, A.; Clore, G.M. Dynamic equilibrium between closed and partially closed states of the bacterial Enzyme I unveiled by solution NMR and X-ray scattering. *Proc. Natl. Acad. Sci. USA*, **2015**, *112*, 11565-70.

[69] Zhang, W.; Collinet, B.; Perrochia, L.; Durand, D.; van Tilbeurgh, H. The ATP-mediated formation of the YgjD-YeaZ-YjeE complex is required for the biosynthesis of tRNA t6A in Escherichia coli. *Nucleic Acids Res*., **2015**, *43*, 1804-17.

[70] Kelley, L.A.; Mezulis, S.; Yates, C.M.; Wass, M.N.; Sternberg, M.J.E. The Phyre2 web portal for protein modeling, prediction and analysis. *Nat. Protocols*, **2015**, *10*, 845-858.

[71] Lapinaite, A.; Simon, B.; Skjaerven, L.; Rakwalska-Bange, M.; Gabel, F.; Carlomagno, T. The structure of the box C/D enzyme reveals regulation of RNA methylation. *Nature*, **2013**, *502*, 519-23.

[72] Hennig, J.; Militti, C.; Popowicz, G.M.; Wang, I.; Sonntag, M.; Geerlof, A.; Gabel, F.; Gebauer, F.; Sattler, M. Structural basis for the assembly of the Sxl-Unr translation regulatory complex. *Nature*, **2014**, *515*, 287-90.

[73] Pilotto, S.; Speranzini, V.; Tortorici, M.; Durand, D.; Fish, A.; Valente, S.; Forneris, F.; Mai, A.; Sixma, T.K.; Vachette, P.; Mattevi, A. Interplay among nucleosomal DNA, histone tails, and corepressor CoREST underlies LSD1-mediated H3 demethylation. *Proc. Natl. Acad. Sci. USA*, **2015**, *112*, 2752-7.

[74] le Maire, M.; Arnou, B.; Olesen, C.; Georgin, D.; Ebel, C.; Moller, J.V. Gel chromatography and analytical ultracentrifugation to determine the extent of detergent binding and aggregation, and Stokes radius of membrane proteins using sarcoplasmic reticulum Ca2+-ATPase as an example. *Nat. Protoc*., **2008**, *3*, 1782-95.

[75] Breyton, C.; Flayhan, A.; Gabel, F.; Lethier, M.; Durand, G.; Boulanger, P.; Chami, M.; Ebel, C. Assessing the conformational changes of pb5, the receptor-binding protein of phage T5, upon binding to its Escherichia coli receptor FhuA. *J. Biol. Chem*., **2013**, *288*, 30763-72.

[76] Abla, M.; Unger, S.; Keller, S.; Bonnete, F.; Ebel, C.; Pucci, B.; Breyton, C.; Durand, G. Micellar and biochemical properties of a propyl-ended fluorinated surfactant designed for membrane-protein study. *J. Colloid. Interface Sci*., **2015**, *445*, 127-36.

[77] Berthaud, A.; Manzi, J.; Perez, J.; Mangenot, S. Modeling detergent organization around aquaporin-0 using small-angle X-ray scattering. *J. Am. Chem. Soc*., **2012**, *134*, 10080-8.

[78] Perez, J.; Koutsioubas, A. Memprot: a program to model the detergent corona around a membrane protein based on SEC-SAXS data. *Acta Crystallogr. D Biol. Crystallogr*., **2015**, *71*, 86-93.

[79] Kaspersen, J.D.; Jessen, C.M.; Vad, B.S.; Srensen, E.S.; Andersen, K.K.; Glasius, M.; Oliveira, C.L.P.; Otzen, D.E.; Pedersen, J.S. Low-Resolution Structures of OmpA-DDM Protein-Detergent Complexes. *Chembiochem*, **2014**, *15*, 2113-2124.

[80] Skar-Gislinge, N.; Simonsen, J.B.; Mortensen, K.; Feidenhans'l, R.; Sligar, S.G.; Moller, B.L.; Bjornholm, T.; Arleth, L. Elliptical structure of phospholipid bilayer nanodiscs encapsulated by scaffold proteins: casting the roles of the lipids and the protein. *J. Am. Chem. Soc*., **2010**, *132*, 13713-22.

[81] Kynde, S.A.; Skar-Gislinge, N.; Pedersen, M.C.; Midtgaard, S.R.; Simonsen, J.B.; Schweins, R.; Mortensen, K.; Arleth, L. Small-angle scattering gives direct structural information about a membrane protein inside a lipid environment. *Acta Crystallogr. D Biol. Crystallogr*., **2014**, *70*, 371-83.

[82] Hansen, S. Bayesian estimation of hyperparameters for indirect Fourier transformation in small-angle scattering. *J. Appl. Crystallogr*., **2000**, *33*, 1415-1421.

[83] Maric, S.; Skar-Gislinge, N.; Midtgaard, S.; Thygesen, M.B.; Schiller, J.; Frielinghaus, H.; Moulin, M.; Haertlein, M.; Forsyth, V.T.; Pomorski, T.G.; Arleth, L. Stealth carriers for low-resolution structure determination of membrane proteins in solution. *Acta Crystallogr. D Biol. Crystallogr*., **2014**, *70*, 317-28.

[84] Kikhney, A.G.; Svergun, D.I. A practical guide to small angle X-ray scattering (SAXS) of flexible and intrinsically disordered proteins. *FEBS Lett*., **2015**, *589*, 2570-7.

[85] Sibille, N.; Bernado, P. Structural characterization of intrinsically disordered proteins by the combined use of NMR and SAXS. *Biochem. Soc. Trans*., **2012**, *40*, 955-62.

[86] De Biasio, A.; de Opakua, A.I.; Cordeiro, T.N.; Villate, M.; Merino, N.; Sibille, N.; Lelli, M.; Diercks, T.; Bernado, P.; Blanco, F.J. p15PAF is an intrinsically disordered protein with nonrandom structural preferences at sites of interaction with other proteins. *Biophys. J*., **2014**, *106*, 865-74.

[87] Schwalbe, M.; Ozenne, V.; Bibow, S.; Jaremko, M.; Jaremko, L.; Gajda, M.; Jensen, M.R.; Biernat, J.; Becker, S.; Mandelkow, E.; Zweckstetter, M.; Blackledge, M. Predictive atomic resolution descriptions of intrinsically disordered hTau40 and alpha-synuclein in solution from NMR and small angle scattering. *Structure*, **2014**, *22*, 238-49.

[88] Lemak, A.; Wu, B.; Yee, A.; Houliston, S.; Lee, H.W.; Gutmanas, A.; Fang, X.; Garcia, M.; Semesi, A.; Wang, Y.X.; Prestegard, J.H.; Arrowsmith, C.H. Structural characterization of a flexible two-domain protein in solution using small angle X-ray scattering and NMR data. *Structure*, **2014**, *22*, 1862-74.

[89] Gruszka, D.T.; Whelan, F.; Farrance, O.E.; Fung, H.K.; Paci, E.; Jeffries, C.M.; Svergun, D.I.; Baldock, C.; Baumann, C.G.; Brockwell, D.J.; Potts, J.R.; Clarke, J. Cooperative folding of intrinsically disordered domains drives assembly of a strong elongated protein. *Nat. Commun*., **2015**, *6*, 7271.

[90] O'Brien, D.P.; Hernandez, B.; Durand, D.; Hourdel, V.; Sotomayor-Perez, A.C.; Vachette, P.; Ghomi, M.; Chamot-Rooke, J.; Ladant, D.; Brier, S.; Chenal, A. Structural models of intrinsically disordered and calcium-bound folded states of a protein adapted for secretion. *Sci. Rep*., **2015**, *5*, 14223.

[91] Capp, J.A.; Hagarman, A..; Richardson, D.C.; Oas, T.G. The statistical conformation of a highly flexible protein: small-angle X-ray scattering of S. aureus protein A. *Structure*, **2014**, *22*, 1184-95.

[92] Bernado, P. Effect of interdomain dynamics on the structure determination of modular proteins by small-angle scattering. *Eur. Biophys. J*., **2010**, *39*, 769-80.

[93] Rambo, R.P.; Tainer, J.A. Characterizing flexible and intrinsically unstructured biological macromolecules by SAS using the Porod-Debye law. *Biopolymers*, **2011**, *95*, 559-71.

[94] Bernado, P.; Blackledge, M. A self-consistent description of the conformational behavior of chemically denatured proteins from NMR and small angle scattering. *Biophys. J*., **2009**, *97*, 2839-45.

[95] Tria, G.; Mertens, H.D.T.; Kachala, M.; Svergun, D.I. Advanced ensemble modelling of flexible macromolecules using X-ray solution scattering. *IUCrJ*., **2015**, *2*, 207-217.

[96] Yang, S.; Blachowicz, L.; Makowski, L.; Roux, B. Multidomain assembled states of Hck tyrosine kinase in solution. *Proc. Natl. Acad. Sci. USA*., **2010**, *107*, 15757-62.

[97] Rozycki, B.; Kim, Y.C.; Hummer, G. SAXS ensemble refinement of ESCRT-III CHMP3 conformational transitions. *Structure*, **2011**, *19*, 109-16.

[98] Bertini, I.; Ferella, L.; Luchinat, C.; Parigi, G.; Petoukhov, M.V.; Ravera, E.; Rosato, A.; Svergun, D.I. MaxOcc: a web portal for maximum occurrence analysis. *J. Biomol. NMR*, **2012**, *53*, 271-80.

[99] Lira-Navarrete, E.; de Las Rivas, M.; Companon, I.; Pallares, M.C.; Kong, Y.; Iglesias-Fernandez, J.; Bernardes, G.J.; Peregrina, J.M.; Rovira, C.; Bernado, P.; Bruscolini, P.; Clausen, H.; Lostao, A.; Corzana, F.; Hurtado-Guerrero, R. Dynamic interplay between catalytic and lectin domains of GalNAc-transferases modulates protein O-glycosylation. *Nat. Commun*., **2015**, *6*, 6937.

[100] Sander, B.; Tria, G.; Shkumatov, A.V.; Kim, E.Y.; Grossmann, J.G.; Tessmer, I.; Svergun, D.I.; Schindelin, H. Structural characterization of gephyrin by AFM and SAXS reveals a mixture of compact and extended states. *Acta Crystallogr. D Biol. Crystallogr*., **2013**, *69*, 2050-60.

[101] Kofinger, J.; Ragusa, M.J.; Lee, I.H.; Hummer, G.; Hurley, J.H. Solution structure of the Atg1 complex: implications for the architecture of the phagophore assembly site. *Structure*, **2015**, *23*, 809-18.

[102] Arnlund, D.; Johansson, L.C.; Wickstrand, C.; Barty, A.; Williams, G.J.; Malmerberg, E.; Davidsson, J.; Milathianaki, D.; DePonte, D.P.; Shoeman, R.L.; Wang, D.; James, D.; Katona, G.; Westenhoff, S.; White, T.A.; Aquila, A.; Bari, S.; Berntsen, P.; Bogan, M.; van Driel, T.B.; Doak, R.B.; Kjaer, K.S.; Frank, M.; Fromme, R.; Grotjohann, I.; Henning, R.; Hunter, M.S.; Kirian, R.A.; Kosheleva, I.; Kupitz, C.; Liang, M.; Martin, A.V.; Nielsen, M.M.; Messerschmidt, M.; Seibert, M.M.; Sjohamn, J.; Stellato, F.; Weierstall, U.; Zatsepin, N.A.; Spence, J.C.; Fromme, P.; Schlichting, I.; Boutet, S.; Groenhof, G.; Chapman, H.N.; Neutze, R. Visualizing a protein quake with time-resolved X-ray scattering at a free-electron laser. *Nat. Methods*, **2014**, *11*, 923-6.

[103] Cammarata, M.; Levantino, M.; Schotte, F.; Anfinrud, P.A.; Ewald, F.; Choi, J.; Cupane, A.; Wulff, M.; Ihee, H. Tracking the structural dynamics of proteins in solution using time-resolved wide-angle X-ray scattering. *Nat. Methods*, **2008**, *5*, 881-6.

[104] Kler, S.; Asor, R.; Li, C.; Ginsburg, A.; Harries, D.; Oppenheim, A.; Zlotnick, A.; Raviv, U. RNA encapsidation by SV40-derived nanoparticles follows a rapid two-state mechanism. *J. Am. Chem. Soc*., **2012**, *134*, 8823-30.

[105] Bordas, J.; Mandelkow, E.M.; Mandelkow, E. Stages of tubulin assembly and disassembly studied by time-resolved synchrotron X-ray scattering. *J. Mol. Biol*., **1983**, *164*, 89-135.

[106] Rocco, M.; Molteni, M.; Ponassi, M.; Giachi, G.; Frediani, M.; Koutsioubas, A.; Profumo, A.; Trevarin, D.; Cardinali, B.; Vachette, P.; Ferri, F.; Pérez, J. A Comprehensive Mechanism of Fibrin Network Formation Involving Early Branching and Delayed Single- to Double-Strand Transition from Coupled Time-Resolved X-ray/Light-Scattering Detection. *J. Am. Chem. Soc*., **2014**, *136*, 5376-5384.

[107] Akiyama, S.; Takahashi, S.; Kimura, T.; Ishimori, K.; Morishima, I.; Nishikawa, Y.; Fujisawa, T. Conformational landscape of cytochrome c folding studied by microsecond-resolved small-angle x-ray scattering. *Proc. Natl. Acad. Sci. USA*., **2002**, *99*, 1329-34.

[108] Pollack, L.; Doniach, S. Time-resolved X-ray scattering and RNA folding. *Methods Enzymol*., **2009**, *469*, 253-68.

[109] West, J.M.; Xia, J.; Tsuruta, H.; Guo, W.; O'Day, E.M.; Kantrowitz, E.R. Time evolution of the quaternary structure of Escherichia coli aspartate transcarbamoylase upon reaction with the natural substrates and a slow, tight-binding inhibitor. *J. Mol. Biol*., **2008**, *384*, 206-18.

[110] Lee, K.K.; Tsuruta, H.; Hendrix, R.W.; Duda, R.L.; Johnson, J.E. Cooperative reorganization of a 420 subunit virus capsid. *J. Mol. Biol*., **2005**, *352*, 723-35.

[111] Preux, O.; Durand, D.; Huet, A.; Conway, J.F.; Bertin, A.; Boulogne, C.; Drouin-Wahbi, J.; Trevarin, D.; Perez, J.; Vachette, P.; Boulanger, P. A Two-State Cooperative Expansion Converts the Procapsid Shell of Bacteriophage T5 into a Highly Stable Capsid Isomorphous to the Final Virion Head. *J. Mol. Biol*., **2013**, *425*, 1999-2014.

[112] Fowler, A.G.; Foote, A.M.; Moody, M.F.; Vachette, P.; Provencher, S.W.; Gabriel, A.; Bordas, J.; Koch, M.H. Stopped-flow solution scattering using synchrotron radiation: apparatus, data collection and data analysis. *J. Biochem. Biophys. Methods*, **1983**, *7*, 317-29.

[113] Provencher, S.W.; Glockner, J. Analysis of the components present in kinetics (or titration) curves. *J. Biochem. Biophys. Methods*, **1983**, *7*, 331-4.

[114] Guinier, A. *X-Ray Diffraction: In Crystals, Imperfect Crystals, and Amorphous Bodies*, Courier Corporation, **1994**.

[115] Aida, T.; Meijer, E.W.; Stupp, S.I. Functional Supramolecular Polymers. *Science*, **2012**, *335*, 813-817.

[116] Gazit, E. Self-assembled peptide nanostructures: the design of molecular building blocks and their technological utilization. *Chem. Soc. Rev*., **2007**, *36*, 1263-1269.

[117] Kumaraswamy, P.; Lakshmanan, R.; Sethuraman, S.; Krishnan, U.M. Self-assembly of peptides: influence of substrate, pH and medium on the formation of supramolecular assemblies. *Soft Matter*, **2011**, *7*, 2744-2754.

[118] Adler-Abramovich, L.; Gazit, E. The Physical Properties of Supramolecular Peptide Assemblies: From building block association to technological applications. *Chem. Soc. Rev*., **2014**, *43*, 6881-6893.

[119] Harrison, R.S.; Sharpe, P.C.; Singh, Y.; Fairlie, D.P. Amyloid peptides and proteins in review. In: *Reviews of Physiology, Biochemistry and Pharmacology* (Amara, S.G.; Bamberg, E.; Fleischmann, B.; Gudermann, T.; Hebert, S.C.; Jahn, R.; Lederer, W.J.; Lill, R.; Miyajima, A.; Offermanns, S.; Zechner, R., Eds.;), Vol. 159, pp. 1-77. Springer Berlin Heidelberg, **2007**.

[120] Do, T.D.; LaPointe, N.E.; Sangwan, S.; Teplow, D.B.; Feinstein, S.C.; Sawaya, M.R.; Eisenberg, D.S.; Bowers, M.T. Factors That Drive Peptide Assembly from Native to Amyloid Structures: Experimental and Theoretical Analysis of [Leu-5]-Enkephalin Mutants. *J. Phys. Chem. B*, **2014**, *118*, 7247-7256.

[121] Laganowsky, A.; Liu, C.; Sawaya, M.R.; Whitelegge, J.P.; Park, J.; Zhao, M.; Pensalfini, A.; Soriaga, A.B.; Landau, M.; Teng, P.K.; Cascio, D.; Glabe, C.; Eisenberg, D. Atomic View of a Toxic Amyloid Small Oligomer. *Science*, **2012**, *335*, 1228-1231.

[122] Gazit, E. Controlling molecular self-assembly: from amyloid oligomerization and therapy to novel biomaterials and technological applications in nanomedicine. *Nanomedicine*, **2014**, *9*, 2433-2436.

[123] Rambaran, R.N.; Serpell, L.C. Amyloid fibrils: Abnormal protein assembly. *Prion*, **2008**, *2*, 112-117.

[124] Knowles, T.P.J.; Buehler, M.J. Nanomechanics of functional and pathological amyloid materials. *Nat. Nano*, **2011**, *6*, 469-479.

[125] Cherny, I.; Gazit, E. Amyloids: Not Only Pathological Agents but Also Ordered Nanomaterials. *Ang. Chem. Intl. Ed*., **2008**, *47*, 4062-4069.

[126] Li, D.; Furukawa, H.; Deng, H.; Liu, C.; Yaghi, O.M.; Eisenberg, D.S. Designed amyloid fibers as materials for selective carbon dioxide capture. *Proc. Natl. Acad. Sci. USA*., **2014**, *111*, 191-6.

[127] Li, D.; Jones, E.M.; Sawaya, M.R.; Furukawa, H.; Luo, F.; Ivanova, M.; Sievers, S.A.; Wang, W.; Yaghi, O.M.; Liu, C.; Eisenberg, D.S. Structure-Based Design of Functional Amyloid Materials. *J. Am. Chem. Soc*., **2014**, *136*, 18044-18051.

[128] Hosseinkhani, H.; Hong, P.D.; Yu, D.S. Self-assembled proteins and peptides for regenerative medicine. *Chem. Rev*., **2013**, *113*, 4837-4861.

[129] Wien, F.; Paternostre, M.; Gobeaux, F.; Artzner, F.; Refregiers, M. Calibration and quality assurance procedures at the far UV linear and circular dichroism experimental station DISCO. *J. Phys*., **2013**, *425*, 122014.

[130] Ardejani, M.S.; Orner, B.P. Materials science. Obey the peptide assembly rules. *Science (New York, N.Y.)*, **2013**, *340*, 561-2.

[131] Fletcher, J.M.; Harniman, R.L.; Barnes, F.R.H.; Boyle, A.L.; Collins, A.; Mantell, J.; Sharp, T.H.; Antognozzi, M.; Booth, P.J.; Linden, N.; Miles, M.J.; Sessions, R.B.; Verkade, P.; Woolfson, D.N. Self-assembling cages from coiled-coil peptide modules. *Science (New York, N.Y.)*, **2013**, *340*, 595-9.

[132] Ghadiri, M.R.; Granja, J.R.; Milligan, R.A.; McRee, D.E.; Khazanovich, N. Self-assembling organic nanotubes based on a cyclic peptide architecture. *Nature*, **1993**, *366*, 324-327.

[133] Vauthey, S.; Santoso, S.; Gong, H.; Watson, N.; Zhang, S. Molecular self-assembly of surfactant-like peptides to form nanotubes and nanovesicles. *Proc. Nat. Acad. Sci*., **2002**, *99*, 5355-5360.

[134] Lu, K.; Jacob, J.; Thiyagarajan, P.; Conticello, V.P.; Lynn, D.G. Exploiting Amyloid Fibril Lamination for Nanotube Self-Assembly. *J. Am. Chem. Soc*., **2003**, *125*, 6391-6393.

[135] Chapman, R.; Danial, M.; Koh, M.L.; Jolliffe, K.A.; Perrier, S. Design and properties of functional nanotubes from the self-assembly of cyclic peptide templates. *Chem. Soc. Rev*., **2012**, *41*, 6023-6041.

[136] Gobeaux, F.; Fay, N.; Tarabout, C.; Meneau, F.; Mériadec, C.; Delvaux, C.; Cintrat, J.C.; Valéry, C.; Artzner, F.; Paternostre, M. Experimental observation of double-walled peptide nanotubes and monodispersity modeling of the number of walls. *Langmuir*, **2013**, *29*, 2739-2745.

[137] Gobeaux, F.; Fay, N.; Tarabout, C.; Mériadec, C.; Meneau, F.; Ligeti, M.; Buisson, D.A.; Cintrat, J.C.; Nguyen, K.M.H.; Perrin, L.; Valéry, C.; Artzner, F.; Paternostre, M. Structural role of counterions adsorbed on self-assembled peptide nanotubes. *J. Am. Chem. Soc*., **2012**, *134*, 723-733.

[138] Gobeaux, F.; Tarabout, C.; Fay, N.; Meriadec, C.; Ligeti, M.; Buisson, D.-A.; Cintrat, J.-C.; Artzner, F.; Paternostre, M. Directing peptide crystallization through curvature control of nanotubes. *J. Pept. Sci*., **2014**, *20*, 508-516.

[139] Steve, P.M.; Warkentin, M.; Chen, H.; Jesse, B.H.; Gillilan, R.E.; Pollack, L.; Thorne, R.E. Breaking the Radiation Damage Limit with Cryo-SAXS. *Biophys. J*., **2014**, *104*, 227-236.

[140] Chen, G.; Zwart, P.H.; Li, D. Component Particle Structure in Heterogeneous Disordered Ensembles Extracted from High-Throughput Fluctuation X-Ray Scattering. *Phys. Rev. Lett*., **2013**, *110*, 195501.

[141] Mendez, D.; Lane, T.J.; Sung, J.; Sellberg, J.; Levard, C.; Watkins, H.; Cohen, A.E.; Soltis, M.; Sutton, S.; Spudich, J.; Pande, V.; Ratner, D.; Doniach, S. *Observation of correlated X-ray scattering at atomic resolution*, 369, **2014**.

Received: July 31, 2015 **Revised: October 25, 2015** **Accepted: October 25, 2015**